nature physics

Article

https://doi.org/10.1038/s41567-024-02498-w

A quantum critical Bose gas of magnons in the quasi-two-dimensional antiferromagnet $YbCl_3$ under magnetic fields

Received: 5 July 2022

Accepted: 28 March 2024

Published online: 09 May 2024

Check for updates

Yosuke Matsumoto[1], Simon Schnierer[1], Jan A. N. Bruin[1], Jürgen Nuss[1], Pascal Reiss[1], George Jackeli[1,2], Kentaro Kitagawa[3] & Hidenori Takagi[1,2,3]

Bose–Einstein condensation (BEC) is a quantum phenomenon in which a macroscopic number of bosons occupy the lowest energy state and acquire coherence at low temperatures. In three-dimensional antiferromagnets, a magnetic-field-induced transition has been successfully described as a magnon BEC. For a strictly two-dimensional (2D) system, it is known that BEC cannot take place due to the presence of a finite density of states at zero energy. However, in a realistic quasi-2D magnet consisting of stacked magnetic layers, a small but finite interlayer coupling stabilizes marginal BEC but such that 2D physics is still expected to dominate. This 2D-limit BEC behaviour has been reported in a few materials but only at very high magnetic fields that are difficult to access. The honeycomb $S = 1/2$ Heisenberg antiferromagnet $YbCl_3$ exhibits a transition to a fully polarized state at a relatively low in-plane magnetic field. Here, we demonstrate the formation of a quantum critical 2D Bose gas at the transition field, which, with lowering the field, experiences a BEC marginally stabilized by an extremely small interlayer coupling. Our observations establish $YbCl_3$, previously a Kitaev quantum spin liquid material, as a realization of a quantum critical BEC in the 2D limit.

XY antiferromagnetism induced by an applied magnetic field H provides a prominent example of Bose–Einstein condensation (BEC)[1,2] in quantum magnets[3–5], which has been established in a wide variety of magnets including spin-singlet dimers $TlCuCl_3$ (refs. 6,7), $BaCuSi_2O_6$ (refs. 8,9) and $S = 1$ magnet with a single ion anisotropy $NiCl_2$-$4SC(NH_2)_2$ (ref. 10). Consider, for example, the case for a Heisenberg antiferromagnet with a nearest-neighbour coupling J in a field H. H along the z-direction polarizes the spins and causes their z-component $<S_z>$ to acquire a finite value. When H is close to the saturation field H_s—that is, near a quantum phase transition to a fully polarized (FP) state—the system effectively becomes an *XY* antiferromagnet with the remaining x- and y-components of the spins, S_x and S_y. As S_x and S_y can be replaced with creation/annihilation operators of bosons, the system can be mapped onto an ensemble of interacting bosons with boson operators b_k^+ and b_k in the momentum k representation, an excitation energy ε_k and an effective chemical potential μ_{eff} (ref. 11), which is described by the following Hamiltonian:

$$H = \sum_k (\varepsilon_k - \mu_{\mathrm{eff}})\, b_k^+ b_k \tag{1}$$

In this mapping, ε_k is determined by the energy dispersion of a tight-binding band with a nearest-neighbour hopping $t = J/2$ measured from the bottom of the band. The effective chemical potential

[1]Max Planck Institute for Solid State Research, Stuttgart, Germany. [2]Institute for Functional Matter and Quantum Technologies, University of Stuttgart, Stuttgart, Germany. [3]Department of Physics, University of Tokyo, Tokyo, Japan. e-mail: Y.Matsumoto@fkf.mpg.de; h.takagi@fkf.mpg.de

https://doi.org/10.1038/s41567-024-02498-w

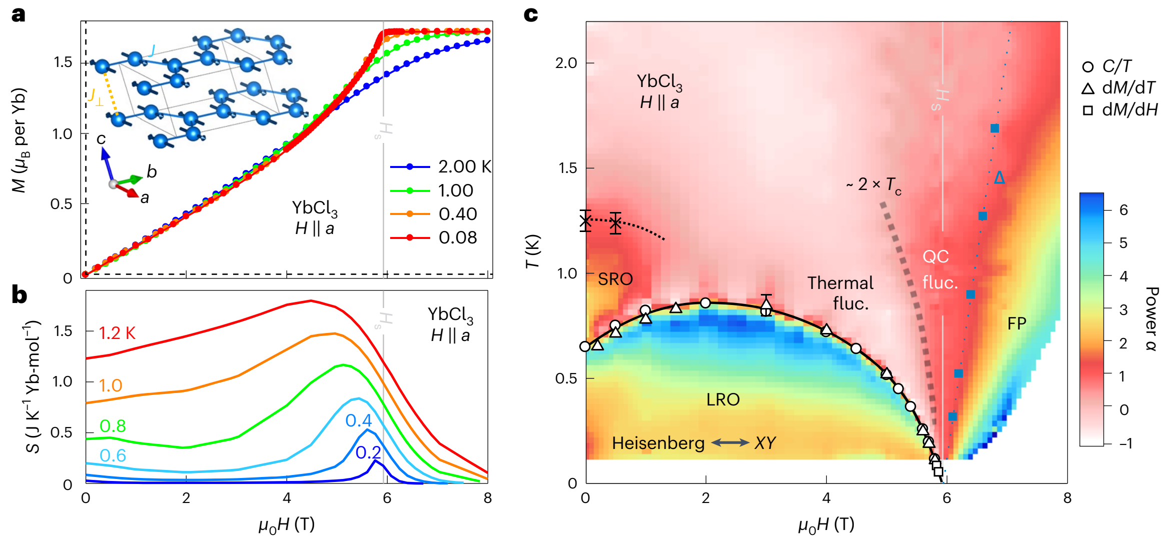

Fig. 1 | Magnetic-field-induced quantum phase transition and *H*–*T* phase diagram for $YbCl_3$. **a**, The magnetization *M*(*H*) curves at different temperatures. The Van Vleck contribution has been subtracted (Supplementary Fig. 1). The inset shows the honeycomb layered structure of $YbCl_3$ (space group *C*12/*m*1)[26,41] with an antiferromagnetic intralayer coupling $J \approx 5$ K and a ferromagnetic interlayer coupling $J_\perp \approx 0.1$ mK. **b**, The magnetic field dependence of entropy at different temperatures. **c**, The *H*–*T* phase diagram. The power α of the *T*-dependent specific heat *C* ($C \propto T^\alpha$ defined as $\alpha(T) \equiv \mathrm{d}\ln C/\mathrm{d}\ln T$) was evaluated by linear fits to ln *C* versus ln *T* for every four data points and is indicated by the colour. The open symbols indicate the T_c of the long-range magnetic ordering, defined by the position of peaks in d*M*/d*T*, *C*/*T* and d*M*/d*H*. The crosses represent the locations of the broad SRO peaks in *C*/*T*. Error bars for circles and crosses are defined by the peak width of the *C*(*T*)/*T* anomaly at 2% below the maximum value, which was determined by fitting 20–30 points around the peak with a polynomial curve. Filled squares indicate the gap size Δ determined by *C*/*T*. A linear fit to Δ is shown with dotted line above H_s. The grey broken line below H_s indicates the onset of the 2D thermal fluctuations above T_c, which is determined as the onset temperature of a rapid increase of *C*/*T* upon cooling (the open arrows in Fig. 2b). fluc., fluctuation.

$$\mu_{\mathrm{eff}} = g\mu_{\mathrm{B}}(H_{\mathrm{S}} - H) - 2U_{\mathrm{eff}} < n >$$

consists of the bare chemical potential controlled by $H_s - H$ and an additional term representing the increase of the mean-field, one-particle energy due to a repulsive boson–boson interaction U_{eff}, which arises from the $JS_z^iS_z^j$ term in the original spin Hamiltonian and is on the order of *J* in the bare form[6,12]. <*n*> is the average number of (hole) bosons per site, which corresponds to the deviation of field-induced magnetization $<S_z>$ from the saturation value. The *XY* ordering below H_s can therefore be treated as a BEC of a low density of interacting bosons in the Hamiltonian. The FP state above H_s has an excitation gap and zero boson density $<n> = 0$ at temperature $T = 0$ and can be regarded as the vacuum state of the bosons. The field-induced quantum phase transition at H_s provides us with a unique opportunity to study a BEC quantum critical point (BEC-QCP).

The nature of the magnetic-field-induced BEC depends sensitively on the dimensionality of the system. In a three-dimensional (3D) magnet, BEC occurs simply as a long-range *XY* ordering. Distinct from the 3D case is a two-dimensional (2D) magnet. It is known that a strictly 2D Bose gas does not experience BEC at a finite temperature, due to the presence of a finite density of states at zero energy and the associated logarithmic divergence of the number integral in the $T = 0$ limit. In the original language of spin, a long-range *XY* ordering in a strictly 2D magnet is suppressed by strong fluctuations down to $T = 0$ (ref. 13). Instead, a quasi-long-range-order (quasi-LRO) emerges: that is, the Berezinskii–Kosterlitz–Thouless (BKT) transition[14–16]. One therefore observes a BKT near H_s in strictly 2D systems, instead of the BEC. The effective boson–boson interaction U_{eff} in 2D is distinct from those in 3D and is subject to logarithmic renormalization as $U_{\mathrm{eff}} = U_0/(-\ln<n>)$, where U_0 is the bare interaction and suppressed appreciably around the QCP[17]. In reality, the bulk '2D magnet' that we investigate experimentally is not a strictly 2D magnet but a quasi-2D magnet, which comprises a stack of strictly 2D magnets with a small but finite interlayer coupling ($J_\perp$). The interlayer coupling should marginally push the system from a BKT transition to a 3D LRO and hence a BEC. Even in such a quasi-2D BEC state, however, 2D physics could be still relevant at temperatures above the temperature scale of $J_\perp$. 2D logarithmic renormalization of U_{eff}, for example, may still be captured. Possible signatures of BKT physics were suggested theoretically[18] and experimentally[19–22] in quasi-2D magnets with intrinsic *XY* character.

It is tempting to explore such a distinct class of marginal BEC in the 2D limit and its BEC-QCP in quasi-2D antiferromagnets under magnetic fields, where we anticipate 2D logarithmic renormalization, 2D quantum and thermal fluctuations with possible signatures of BKT physics and an interplay with 3D physics arising from a minute interlayer coupling $J_\perp$. So far, despite the long history of BEC and BEC-QCP in antiferromagnets, such exploration for the 2D limit has been limited due to the lack of an appropriate model system. The quasi-2D dimer system $BaCu_2Si_2O_6$ shows a magnetic-field-induced BEC above the QCP where a finite magnetization emerges. The reduction of the effective interlayer coupling due to frustration was argued to play a vital role[9]. The linear decrease of the transition temperature T_c as a function of the magnetic field around QCP, which is expected for a BEC in the 2D limit[23], suggests the presence of 2D quantum fluctuations. However, the frustration scenario was challenged by the later observation of ferromagnetic interlayer coupling. The presence of two types of dimers does not allow for a straightforward interpretation of the critical behaviour[24]. More importantly, signatures of '2D' critical fluctuations other than the linear scaling of transition temperature and underlying boson–boson interactions have not yet been unveiled, in contrast to the 3D case (for example, $TlCuCl_3$ (ref. 6) and $NiCl_2$-$4SC(NH_2)_2$ (ref. 25)), partly due to the very high magnetic field needed to reach the QCP. To capture the BEC criticality in the 2D limit experimentally, a material system with an easily accessible QCP is highly desired, where one can probe 2D quantum and thermal fluctuations and underlying interactions through other thermodynamic parameters in addition to T_c.

The pseudospin 1/2 Heisenberg antiferromagnet $YbCl_3$ may be an ideal system for the exploration of the quasi-2D BEC-QCP.

 https://doi.org/10.1038/s41567-024-02498-w

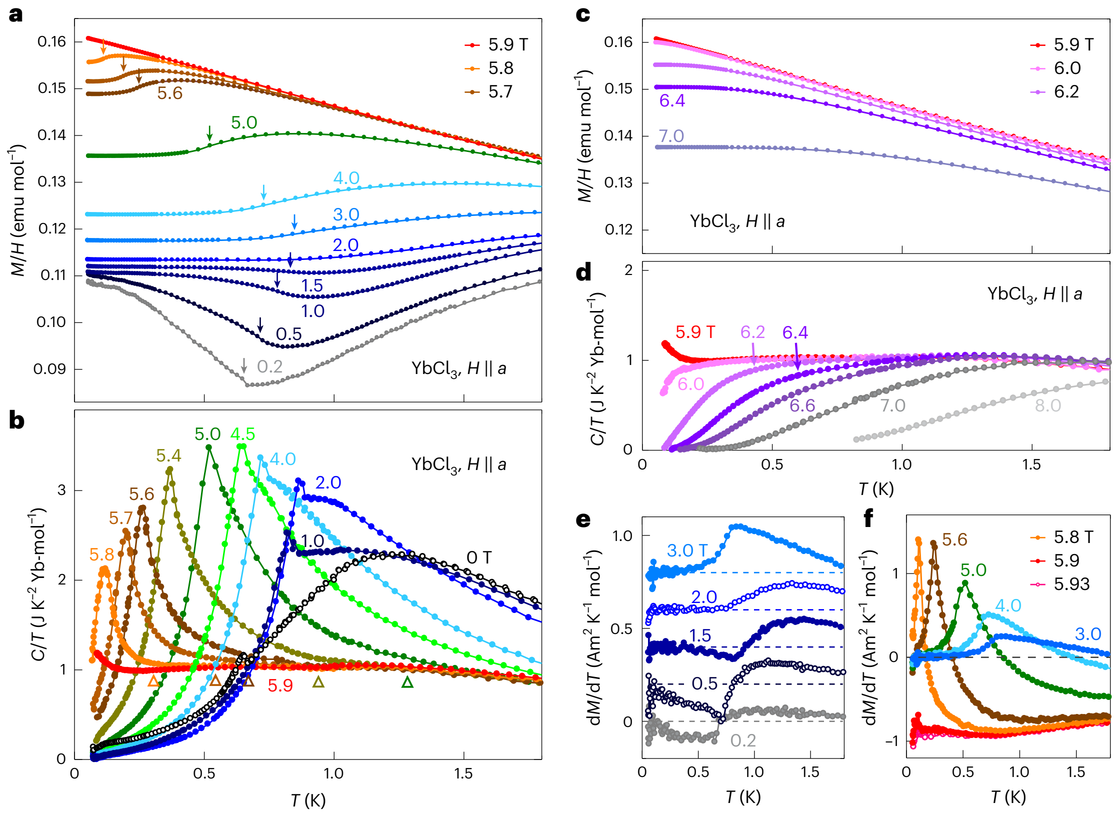

Fig. 2 | Temperature dependence of magnetization *M*(*T*) and specific heat *C*(*T*) at different magnetic fields. a,**c**, *T*-dependent *M*/*H* for $H \le H_s$ (**a**) and $H \ge H_s$ (**c**). The arrows in **a** represent T_c determined from the singularity in d*M*/d*T* (**e**,**f**). **b**,**d**, *T*-dependent *C*/*T* for $H \le H_s$ (**b**) and $H \ge H_s$ (**d**). Open triangles in **b** mark the onset temperature for thermal fluctuations towards T_c, where *C*/*T* starts to deviate from the constant behaviour upon cooling. **e**,**f**, *T*-dependence of the derivative of magnetization d*M*/d*T* below (**e**) and above (**f**) 3 T, respectively. The data at each field in **e** are shifted by 0.2 Am^2 K^{-1} mol^{-1} for clarity.

The material has the 2D honeycomb-based structure shown in the inset of Fig. 1a (ref. 26) and was earlier suggested as a possible Kitaev magnet with anisotropic bond-dependent couplings[27]. Recent inelastic neutron-scattering measurements, however, revealed that the system is a quasi-2D Heisenberg antiferromagnet with an almost isotropic in-plane nearest-neighbour coupling $J \approx 5$ K (= 0.42 meV) and a very small interlayer coupling $|J_\perp/J| \approx 3 \times 10^{-5}$ (ref. 28). Recent quantum Monte Carlo (QMC) simulations on this system indicate a ferromagnetic interlayer coupling at least smaller than $|J_\perp/J| \approx 2 \times 10^{-3}$ (ref. 29), consistent with the estimate from the inelastic neutron-scattering measurement[28]. $J_\perp$ is therefore extremely small, likely of the order of 0.1 mK and at most 10 mK, rendering this system ideal to explore a BEC close to the 2D limit. Specific heat and neutron diffraction measurements indicate the occurrence of a 3D long-range Néel ordering at $T_N = 0.6$ K (ref. 30) with an ordered moment of ~1 μ_B (refs. 27,28,30), which is stabilized by the small $J_\perp$. Alternating-current susceptibility measurements indicate a magnetic-field-induced transition to a FP state at $H_s = 6$ and 9.5 T with the field applied in and out of plane, respectively[27], which we argue to be a quasi-2D BEC-QCP.

We therefore have explored the quasi-2D BEC-QCP in $YbCl_3$ with the in-plane magnetic field *H* as a tuning parameter of the quantum phase transition. At the QCP, we identified clear signatures of BEC quantum critical fluctuations in the 2D limit, which manifest themselves as the formation of a highly mobile, correlated 2D Bose gas in the dilute limit, where the effective boson–boson interaction is an order of magnitude smaller than those of its 3D analogues due to the expected logarithmic renormalization of boson–boson interaction. The finite temperature transitions below the saturation field H_s (that is, the QCP) can be described as a BEC induced by an extremely small interlayer coupling $J_\perp$ of ~0.1 mK.

Heisenberg-like to *XY*-like crossover and the QCP

Single crystals of $YbCl_3$ used in this study were grown by a chemical vapour-transport technique (Methods). The magnetic field was always applied along the in-plane *a*-direction, perpendicular to one of the honeycomb bonds. The magnetization *M* shown in Fig. 1a reaches the saturation moment $M_s = 1.72\ \mu_B$ per Yb around $H_s \approx 5.9$ T. The saturation field in the $T = 0$ limit, which marks the quantum phase transition, was estimated as $H_s = 5.93 \pm 0.01$ T from the crossing point of d*M*/d*H* curves at 0.05 and 0.08 K (Supplementary Information and Supplementary Fig. 1).

At zero field, the specific heat divided by temperature *C*/*T* shown in Fig. 2b exhibits a broad peak from a short-range 2D antiferromagnetic correlation around 1.2 K, followed by a tiny but sharp peak from the long-range 3D Néel ordering at $T_c = 0.65$ K, fully consistent with the previous studies[27,30]. Weak signature of the Néel order is also present in *M*(*T*), which is more clearly visualized in the temperature derivative d*M*/d*T* (Fig. 2e,f). Upon applying *H*, T_c first increases until $H_p \approx 2$–3 T and then decreases to zero at the saturation field $H_s = 5.93$ T (refs. 27,30). This evolution is summarized in the phase diagram shown in Fig. 1c. The initial increase of T_c indicates the suppression of fluctuations along the field direction and the crossover of symmetry from Heisenberg-like to *XY*-like, as discussed in a class of low-dimensional Heisenberg magnets[31,32]. The suppression of fluctuations can indeed be captured by the initial decrease of the isothermal entropy up to H_p at temperatures below 0.8 K in Fig. 1b, as well as a negative slope $dM/dT|_H (= dS/dH|_T)$ in the same *H*- and *T*-range in Fig. 2a,e.

Above $H_p \approx 2$–3 T, the system should have predominant *XY* character. Reflecting this change of symmetry, the anomalies at T_c in *C*/*T* and *M* show qualitatively different behaviour from that of the zero-field limit. In *C*/*T*, the small λ-like peak associated with LRO and the broad peak associated with short-range ordering (SRO) merge at higher fields into one sharp cusp-like peak (Fig. 2b). The weak anomaly in dM/dT at low fields changes to a cusp-like anomaly near H_p (Fig. 2e,f). As H increases further towards H_s, the LRO with XY character is suppressed due to the reduced S_x and S_y degrees of freedom and T_c decreases to zero (Fig. 1c). In this field region near H_s, the LRO with XY character is described as a quasi-2D BEC induced by interlayer coupling, as we will discuss below. In the language of bosons, the suppression of the quasi-2D BEC upon approaching the QCP at H_s can be described by a decrease of the boson density to zero.

Above H_s, we observe thermally activated behaviours of C and $(M_s - M)/M_s$ at low temperatures (Supplementary Fig. 4a,b), indicating the emergence of a gap in the magnetic (boson) excitations in the FP state. The extracted activation energy Δ, as shown in Fig. 1c and Supplementary Fig. 4c, increases linearly from H_s as roughly $g\mu_B(H_s - H)$, where $g \approx 3.67$ is the g-factor for $S = 1/2$ pseudospins (Supplementary Information). In the language of bosons, $g\mu_B(H_s - H)$ corresponds to the energy between the bare chemical potential μ and the bottom of the band and sets the excitation gap above H_s. These behaviours above H_p indicate that the honeycomb antiferromagnet $YbCl_3$ under magnetic field is an excellent arena to explore a quasi-2D BEC and the associated BEC-QCP.

2D-limit BEC critical fluctuations at the QCP

At the saturation field H_s—that is, the QCP—we indeed find evidence for quantum fluctuations predicted for a BEC-QCP in the 2D limit. The critical behaviours of $C(T)$, $M(T)$ and $T_c(H)$ at a field-induced BEC-QCP in d dimensions are predicted to be $C \propto T^{d/2}$, $M_s - M \propto T^{d/2}$ and $T_c(H) \propto (H_s - H)^{2/d}$ (refs. 3,23,33,34). In the 3D BEC systems such as $TlCuCl_3$ (ref. 6) and $NiCl_2$-4SC$(NH_2)_2$ (ref. 25), the critical exponents with $d = 3$ were firmly established at the BEC-QCP. As summarized in Figs. 2b,c and 3a,b, in stark contrast to 3D model systems, all three parameters of $YbCl_3$, C, M and T_c, closely follow the expected critical behaviour in the 2D ($d = 2$) limit at H_s. C is linear in T with a coefficient $\gamma = C/T \approx 1$ J K^{-2} Yb-mol^{-1} over a wide T range below ~1.2 K. M decreases linearly with T from the saturation moment as $M = M_s - M_s(T/T_0)$ with $T_0 = 11$ K. In the language of bosons, the boson density $<n> \equiv (M_s - M)/M_s = T/T_0$ goes to zero at $T = 0$. T_c scales linearly with $H_s - H$ near the critical point H_s. These quantum critical behaviours can be utilized as markers for quantum fluctuations. The power exponent of $C(T)$, $\alpha(T) \equiv$ d ln C/d ln T, is indicated as a colour contour map on the H–T phase diagram in Fig. 1c. The red region for $\alpha \approx 1$, which represents BEC criticality in the 2D limit, spreads like a fan from the QCP at H_s. The contour map of dM/dT yields essentially the same quantum critical region (Supplementary Information). The fanlike spread is indeed the canonical behaviour of a quantum critical regime around the QCP, which confirms that the critical exponents, which are consistent with a BEC-QCP in the 2D limit, arise from quantum critical fluctuations. The 2D quantum critical behaviour is observed at least down to our lowest temperature of measurements, $T = 50$ mK. We note that 50 mK is only 1% of $J = 5$ K but still orders of magnitude higher than the energy scale of $J_\perp$, which is on the order of 0.1 mK based on previous neutron-scattering studies and our analysis below. A substantial part of the 3D critical behaviour originating from the small $J_\perp$ is very likely hidden in the low-temperature limit below experimentally accessible temperatures.

An interacting 2D Bose gas in the dilute limit at the QCP

The quasi-2D BEC-QCP lies at the limit of zero boson density, where the system hosts a dilute and therefore weakly interacting boson gas produced by thermal excitations at a finite temperature. Let us consider a 2D boson gas with a constant density of states $D(E) = D$ and an effective chemical potential $\mu_{\rm eff} = g\mu_B(H_s - H) - 2U_{\rm eff}<n>$, as shown in Fig. 3c. For a tight-binding model on the 2D honeycomb lattice with nearest-neighbour hopping $t = J/2$, $D = \sqrt{3}/2\pi J$ at the bottom of the band (energy $E = 0$) (Supplementary Information). From the number integral with the Bose function, $<n>$ and $\mu_{\rm eff}$ are related by the following equation:

$$\exp\left(-<n>/Dk_B T\right) + \exp\left(\mu_{\rm eff}/k_B T\right) = 1 \qquad (2)$$

where k_B is the Boltzmann constant. At the QCP with $H = H_s$, $\mu_{\rm eff} = -2U_{\rm eff}<n>$. Equation (2) then requires $<n>$ and hence $\mu_{\rm eff}$ to be linear in T, in accord with the BEC critical behaviour of $<n>$ in the 2D limit. The experimentally obtained T-linear boson density from M in Fig. 3a, $<n> = T/T_0$ ($T_0 = 11$ K $= 2.2J$), yields $U_{\rm eff} = 1.2$ K $= 0.24J$ from equation (2). It is known that the free 2D Bose gas ($U_{\rm eff} = 0$) with zero chemical potential has a T-linear $C(T)$ at low temperatures with a linear coefficient $\gamma = (\pi^2/3)k_B{}^2D$, the same expression as that of a free Fermi gas. With $D = \sqrt{3}/2\pi J$ and $J = 5$ K, the free boson γ is 1.5 J K^{-2} mol^{-1}. We find that the T-linear negative shift of the chemical potential from zero, $\mu_{\rm eff} = -2U_{\rm eff}<n> = -0.21k_BT$, reduces the γ value from the free boson value to 0.99 J K^{-2} mol^{-1}, in excellent agreement with the experimental data (Supplementary Information). These results firmly justify the estimate of $U_{\rm eff}$ and $\mu_{\rm eff}$ and, more importantly, the 2D Bose gas description. The BEC quantum criticality in the 2D limit manifests itself as the formation of an interacting 2D Bose gas at the zero-density limit.

$U_{\rm eff} = 0.24J$ is an order of magnitude smaller than those estimated for prototypical 3D BEC systems, $5J$ for $TlCuCl_3$ (refs. 35,36) and $3J$ for $NiCl_2$-4SC$(NH_2)_2$ (ref. 37). We argue that this represents the logarithmic renormalization of boson–boson scattering U_0 unique to 2D, $U_{\rm eff} \approx -U_0/\ln<n>$ (ref. 17) and mirrors the 2D character of quantum critical Bose gas in $YbCl_3$. The 2D renormalization alone would bring $U_{\rm eff}$ to zero at the quantum critical point due to the logarithmic divergence. We argue that $U_{\rm eff}$ stays at a finite value ~$0.24J$ even at the QCP here due to the weak three-dimensionality associated with the interlayer coupling $J_\perp$, which suppresses the logarithmic singularity at the bottom of the band, as we discuss later. The cut-off of logarithmic divergence is roughly estimated as $U_c \approx -U_0/\ln(J_\perp/J)$, which suggests $-\ln(J_\perp/J) \approx 10$ for $YbCl_3$.

BEC due to a finite interlayer coupling $J_\perp$

Lowering the applied magnetic field below H_s, which corresponds to boson doping, clear anomalies indicative of a phase transition emerge in the T-dependent $C(T)$ and $M(T)$ at $T_c(H)$, as shown in Fig. 2. We found that $T_c(H)$ can be quantitatively described as a BEC of 3D system by introducing an extremely small interlayer coupling $J_\perp$ to a purely 2D band, which implies that the transitions are a long-range magnetic ordering stabilized by the interlayer coupling rather than the BKT transition for 2D. The presence of a small interlayer coupling $J_\perp$ rounds the bottom of the purely 2D band and produces a corresponding $\sqrt{E}$-dependent density of states, as expected in 3D, within the extremely narrow energy range set by $J_\perp$ (Fig. 3c). The continuously vanishing density of states at $E = 0$ prevents a logarithmic divergence of the number integral and hence gives rise to a BEC at a finite temperature. We approximate the rounding of the constant 2D density of states $D(E) = D$ near the bottom of the band by introducing an energy cut-off E_c below which $D(E)$ is replaced with the 3D density of states, $\sqrt{E/E_c}$. E_c is of the order of $J_\perp$, roughly 2–$3J_\perp$. By setting $\mu_{\rm eff} = 0$ in the number integral, a BEC occurs at $<n_c>$ and $T_{\rm BEC}$ satisfying

$$<n_c> \approx Dk_B T_{\rm BEC}\left(-\ln\left(\frac{k_B T_{\rm BEC}}{E_c}\right) + 2\right). \qquad (3)$$

The first and second terms in equation (3) come from the 2D boson density above E_c and the small 3D contribution below E_c, respectively. In Fig. 3a, we overlay equation (3) with $D = \sqrt{3}/2\pi J$, $J = 5$ K and $E_c = 0.2$ mK ($= 2J_\perp$ for $J_\perp/J = 2 \times 10^{-5}$) as a solid line. The predicted $<n_c>$ and $T_{\rm BEC}$ reasonably reproduce the experimentally observed T_c and $<n_c>$ (arrows in Fig. 3a). This close agreement clearly indicates that the magnetic

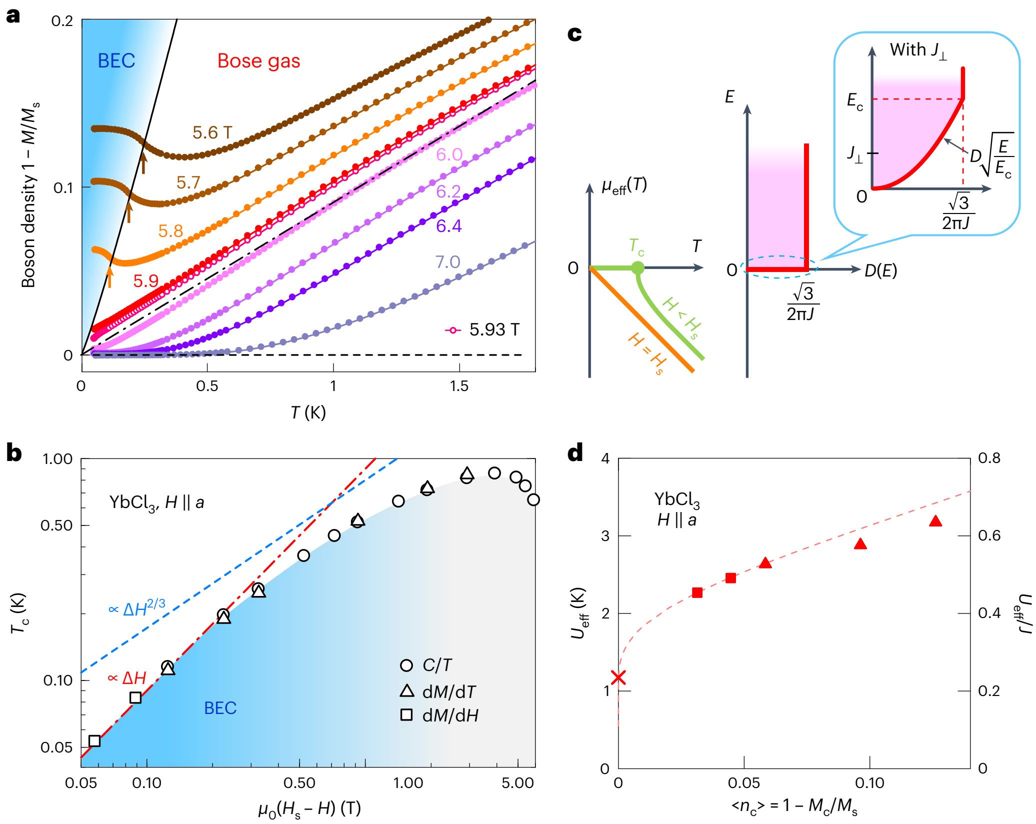

Fig. 3 | Quantum critical behaviour of magnetization $M(T)$ and $T_c(H)$, and quasi-2D Bose gas model. a, Temperature dependence of boson density $<n> = 1 - M/M_s$ for various magnetic fields H around the QCP. The dashed line represents $<n> = T/T_0$, and $T_0 = 11$ K = 2.2J. The arrows indicate T_c determined from the peak in dM/dT (Fig. 2e,f). The solid line represents $<n_c> = Dk_BT_{BEC}(-\ln(k_BT_{BEC}/E_c) + 2)$ with a cut-off energy $E_c = 0.2$ mK and $D = \sqrt{3}/2\pi J$ for $J = 5$ K (Fig. 3c). **b**, Full logarithmic plot of T_c as a function of $H_s - H$, with $H_s = 5.93$ T. The dashed and the broken lines represent $T_c \propto (H_s - H)$ and $(H_s - H)^{2/3}$ expected for 2D and 3D, respectively. **c**, The dilute Bose gas model used to analyse $C(T)$ and $M(T)$ around the QCP. The density of states $D(E)$ for the 2D honeycomb tight-binding model has a bandwidth of 3J and a finite value at $E = 0$, $D = \sqrt{3}/2\pi J$. In the presence of a small interlayer coupling $J_\perp (\ll J)$, a 3D density of states with $D(E)$ proportional to $\sqrt{E}$ shows up at the bottom of the band over the scale of $J_\perp$. The effective chemical potential $\mu_{eff}(T) = g\mu_B(H_s - H) - 2U_{eff}<n>$ approaches $E = 0$ linearly with T at $H = H_s$. For $H < H_s$, μ_{eff} goes to zero at a finite temperature due to the suppression of the logarithmic divergence by the 3D DOS below E_c. **d**, The effective boson–boson interaction U_{eff} versus the critical boson density $<n_c>$. U_{eff} at $<n_c> \to 0$ ($H = H_s$, cross) was estimated from the linear T-dependence of $<n>$. For $H < H_s$, U_{eff} was estimated from $<n_c>$ at $T_c(H)$ in **a** (triangles) and at $H_c(T)$ in Supplementary Fig. 1c (squares) by using $U_{eff} = g\mu_B(H_s - H)/2<n_c>$. The broken line represents the $<n_c>$ dependence of U_{eff} with 2D logarithmic renormalization and a cut-off by $J_\perp$, phenomenologically expressed by $U_{eff} = -U_0(1/\ln<n_c> + 1/\ln(J_\perp/J))$. A bare boson–boson interaction $U_0 = 6$ K = 1.2J and $J_\perp/J = 2 \times 10^{-5}$ are used.

ordering near the QCP is described as a BEC stabilized by a very small interlayer coupling $J_\perp$ of the order of $10^{-5}J$. The extremely small $J_\perp$ compared to J implies that $YbCl_3$ is very close to the 2D limit. We note that the estimate of interlayer coupling is fully consistent with that in a previous neutron-scattering study[28].

At the BEC, the chemical potential $\mu_{eff} = g\mu_B(H_s - H) - 2U_{eff}<n_c> = 0$. This gives an estimate of the effective interaction $U_{eff} = g\mu_B(H_s - H)/2<n_c>$ for $H < H_s$, which is plotted as a function of $<n_c>$ in Fig. 3d. With $<n_c> \to 0$, U_{eff} only weakly decreases to $U_{eff} \approx 0.2J$, which is estimated from the analysis of a 2D quantum critical Bose gas at $H = H_s$. The decrease can be fitted reasonably by $U_{eff} = -U_0(1/\ln<n_c> + 1/\ln(J_\perp/J))$ with $U_0 = 6$ K = 1.2J and $J_\perp/J = 2 \times 10^{-5}$ with 2D logarithmic renormalization and 3D cut-off, as seen by the dotted line in Fig. 3d. U_0 is smaller than but reasonably close to the $U_{eff} = 3$–$5J$ estimated for the canonical 3D BEC systems. Note that $U_{eff} = -U_0/\ln<n_c>$ goes to 0 with $<n_c> \to 0$ but stays a finite U_{eff} of ~0.2J at $<n_c> \approx 0$, which we discussed as a cut-off by the interlayer coupling $J_\perp$. These observations firmly establish the presence of 2D logarithmic renormalization, one of the hallmarks of 2D physics.

Thermal fluctuations in the 2D limit

Reflecting the proximity of the system to the 2D limit, clear signatures of 2D thermal fluctuations are observed above T_c in the specific heat data. In the specific heat power $\alpha(T)$ map in Fig. 1c, the red region of 2D quantum critical behaviour with $\alpha \approx 1$ crosses over to a white region with $\alpha < 1$ with lowering temperature. The white area that extends down to T_c corresponds to the accelerated increase of $C(T)/T$ from a T-independent behaviour upon approaching T_c in Fig. 2b, which marks the region of thermal fluctuations. It spreads over a wide range of temperatures, from as high as ~2T_c (dotted line in Fig. 1c) down to T_c, which points to the 2D character of the thermal fluctuations. Below T_c, we see a decrease of $C(T)/T$ and a corresponding positive power α that decreases eventually to ~2. As the lowest temperature ~100 mK is still higher than 0.5T_c in the critical region near H_s (>5.5T), it is difficult to extract the low-T limit of α and to discuss the dimensionality of fluctuations below T_c.

Because the system is essentially an XY magnet near the QCP and in the 2D limit, the 2D fluctuations observed above and below T_c may carry certain characteristics of a BKT transition for the strictly 2D case. It is tempting to infer here that the hypothetical BKT transition temperature T_{BKT} in the $J_\perp = 0$ limit is very likely close to the observed BEC transition temperature T_c. Theoretically, it was shown for classical spins that the long-range ordering temperature T_c for a small $J_\perp$ is only slightly above T_{BKT} (ref. 38). QMC simulations of a $S = 1/2$ Heisenberg antiferromagnet on a purely 2D square lattice (not honeycomb lattice) under magnetic fields near the saturation field H_s (ref. 39) give

https://doi.org/10.1038/s41567-024-02498-w

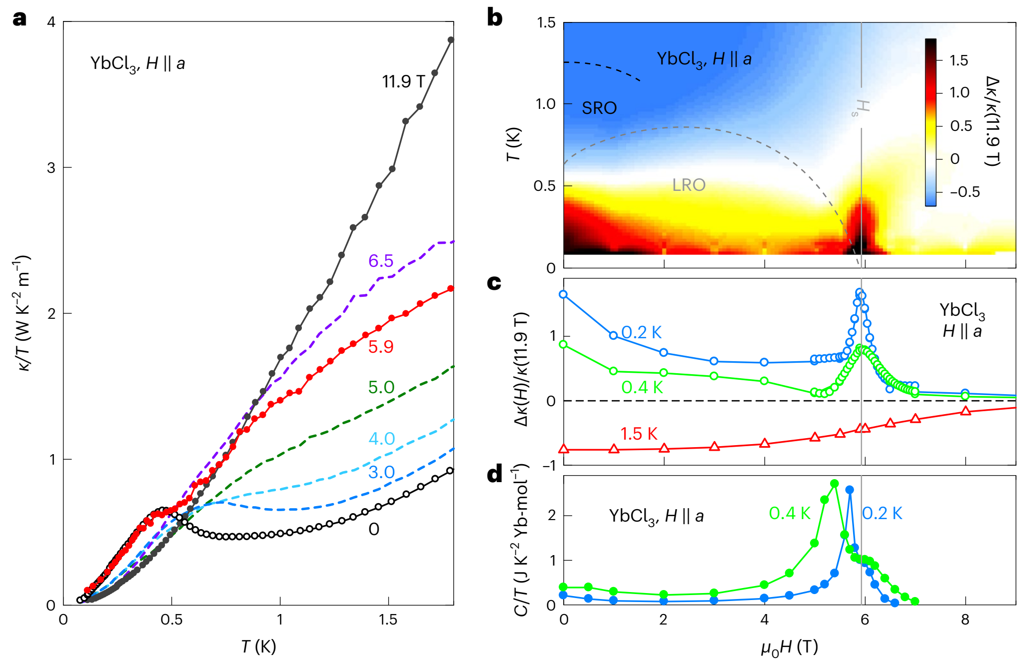

Fig. 4 | Enhancement of thermal conductivity κ at the quantum critical point H_s. a, Thermal conductivity κ/T as a function of temperature T under magnetic fields up to 11.9 T. **b**, The normalized excess thermal conductivity $\Delta\kappa(H)/\kappa(11.9\ \mathrm{T}) = [\kappa(T,H) - \kappa(T, 11.9\ \mathrm{T})]/\kappa(T, 11.9\ \mathrm{T})$ plotted as a colour map on the magnetic field H and the temperature T plane. The excess conductivity $\Delta\kappa(H) = \kappa(H) - \kappa(11.9\ \mathrm{T})$ is the deviation from $\kappa(T)$ at 11.9 T. $\kappa(11.9\ \mathrm{T})$ data can be regarded as a phonon-only contribution to κ in the absence of scattering by magnetic excitations. **c**, The H-dependence of $\Delta\kappa(H)/\kappa(11.9\ \mathrm{T})$ at 0.2, 0.4 and 1.5 K. **d**, The H-dependence of $C(H)/T$ at 0.2 and 0.4 K.

an estimate of the BKT transition temperature $T_{\mathrm{BKT}}/J \approx 1 - H/H_s$, which is indeed reasonably close to the experimentally observed BEC transition temperatures T_c in Fig. 1c.

Highly mobile nature of 2D Bose gas at the QCP

The interacting 2D Bose gas at the QCP is highly mobile at low temperatures, very likely due to the reduced boson–boson interactions in the dilute and 2D limit, which shows up as a singular enhancement of thermal conductivity $\kappa(T)$ at H_s. Figure 4a shows the temperature dependence of κ/T. At the highest measured field of 11.9 T, the heat flow carried by magnetic excitations and the scattering of phonons by magnetic excitations are negligibly small below 2 K, as the gap for magnetic excitations is well developed (»2 K in Fig. 1c). $\kappa(T)$ at 11.9 T is therefore a reference for the maximum phonon thermal conductivity in the absence of scattering by magnetic excitations. $\kappa(T)$ at high temperatures above ~0.6 K decreases monotonically with lowering H from 11.9 T, reflecting the phonon-dominated thermal transport in the corresponding temperature range and the increase of magnetic excitations to scatter phonons due to the suppression of the magnetic excitation gap. At lower temperatures below ~0.5 K, $\kappa(T)$ is larger than that at 11.9 T, the maximum phonon thermal conductivity, which indicates the presence of additional contributions other than the phonon contribution, naturally those from magnetic excitations. We plot the normalized differential thermal conductivity $\Delta\kappa/\kappa(11.9\ \mathrm{T}) \equiv [\kappa(T,H) - \kappa(T, 11.9\ \mathrm{T})]/\kappa(T, 11.9\ \mathrm{T})$ as a colour contour map on the H–T phase diagram in Fig. 4b, where the positive contribution indicates the excess thermal conductivity originating from the magnetic heat carriers. A singular positive $\Delta\kappa$ emerges up to ~0.5 K as a vertical red spike with a width of ~0.4 T around H_s in Fig. 4b, indicating that the magnetic contribution of thermal conductivity at low temperatures peaks sharply at H_s independent of T. This can be confirmed in the isotherm in Fig. 4c.

The thermal conductivity of 2D magnetic excitations is expressed as $\kappa_{\mathrm{mag}} = (1/2)C_{\mathrm{mag}}\langle v_{\mathrm{mag}}\rangle l_{\mathrm{mag}}$, where C_{mag}, v_{mag} and l_{mag} are the specific heat, the velocity and the mean free path of magnetic excitations, respectively. $C_{\mathrm{mag}}(H) \approx C(H)$ at low temperatures shows a peak at the magnetic transition field $H_c(T)$, as in Fig. 4d, which moves away to a lower field from H_s with increasing T and is distinct from the position of the $\Delta\kappa$ peak always at H_s. The singular enhancement of magnetic thermal conductivity $\Delta\kappa$ should therefore be dominated by the enhancement of $\langle v_{\mathrm{mag}}\rangle l_{\mathrm{mag}}$ at H_s. As $\langle v_{\mathrm{mag}}\rangle \approx \sqrt{2mk_BT}$ (m, boson mass) does not strongly depend on H around H_s, $l_{\mathrm{mag}}(H)$ must be enhanced drastically in a very narrow field region near the QCP. At $T = 0.2$ K, the peak value $\Delta\kappa/T \approx 0.13\ \mathrm{W\,K^{-2}\,m^{-1}}$ at $H = H_s$ represents a lower bound for the magnetic contribution κ_{mag}/T, as the phonon contribution $\kappa_{\mathrm{ph}}(T)$ should be suppressed from the maximum phonon contribution $\kappa(T, 11.9\ \mathrm{T})$ in the presence of scattering by magnetic excitations. We estimate a thermal velocity $\langle v_{\mathrm{mag}}\rangle$ of 62 m s^{-1} using a boson mass of 1,570 m_e at the bottom of the honeycomb tight-binding band with a hopping $t = J/2 = 2.5$ K. From $\Delta\kappa T^{-1}$ and $\langle v_{\mathrm{mag}}\rangle$ together with $C_{\mathrm{mag}}/T \approx C/T = 1\ \mathrm{J\,mol^{-1}\,K^{-2}}$ at $H = H_s$, we estimate a lower bound for the mean free path of 2D quantum critical bosons as long as $l_{\mathrm{mag}} \approx 0.3$ µm, which indicates the highly mobile nature of 2D bosons. We were not able to conduct a more detailed and deeper analysis of $\kappa_{\mathrm{mag}}(T)$ and $l_{\mathrm{mag}}(T)$ because of the difficulty in estimating quantitatively the suppressed phonon contribution $\kappa_{\mathrm{ph}}(T)$ in the presence of magnetic excitations (see Supplementary Information for further details). We note that in the red-spike region of the rapid enhancement of $\Delta\kappa$ in Fig. 4b, the number of bosons $\langle n\rangle$ is less than 0.1. We argue that the low boson density $\langle n\rangle$ around H_s reduces the dominant boson–boson scattering represented by $2U_{\mathrm{eff}}\langle n\rangle$ and makes the quantum critical 2D Bose gas highly mobile, which drastically enhances $\Delta\kappa$. The 2D logarithmic suppression of boson–boson scattering U_{eff} may further enhance $\Delta\kappa$ around the QCP. An increase of κ around a QCP was also observed in the 3D magnetic BEC system, $NiCl_2$-$4SC(NH_2)_2$, at very low temperatures[40]. The κ peak as a function H around the QCP, however, is appreciably broader than the present 2D case, if normalized by the field scale of H_s, and appears to be closely correlated with the $C(H)$ peak in contrast to the present 2D case. In this 3D analogue, the dominant scattering of bosons is indeed ascribed to static defects (disorder)[40] rather than boson–boson interactions in the temperature range of investigation.

In summary, we identified a 2D-limit BEC quantum criticality in the honeycomb quasi-2D Heisenberg antiferromagnet $YbCl_3$ under magnetic fields around the saturation field H_s, where a magnetic-field-induced quantum phase transition to the FP state takes place. At H_s, the QCP, the system behaves as a highly mobile dilute 2D gas of bosons in the density $\langle n \rangle = 0$ limit, with the critical exponents of specific heat $C(T)$ and magnetization $M(T)$ predicted for the BEC-QCP in the 2D limit. Lowering the magnetic field to $H < H_s$, an extremely weak interlayer coupling $J_\perp \approx 10^{-5}J$ marginally stabilizes a 3D LRO below T_c, which can de described quantitatively as a BEC. Reflecting the 2D-limit nature, 2D quantum and thermal fluctuations are captured clearly above T_c. A small boson–boson interaction U_{eff} of ~0.2J, one order of magnitude smaller than those in 3D analogues, is observed at the QCP, which increases only weakly with lowering H from the QCP, namely boson doping. The drastic suppression and the weak H-dependence can be quantitatively described as the logarithmic renormalization of the bare boson–boson interaction unique to 2D. $YbCl_3$ is an ideal arena to explore the physics of 2D interacting hard-core bosons.

Online content

Any methods, additional references, Nature Portfolio reporting summaries, source data, extended data, supplementary information, acknowledgements, peer review information; details of author contributions and competing interests; and statements of data and code availability are available at https://doi.org/10.1038/s41567-024-02498-w.

References

1. Bose, S. N. Plancks gesetz und lichtquantenhypothese. *Z. Phys.* **26**, 178–181 (1924).
2. Einstein, A. Quantentheorie des einatomigen idealen gases. *Sitzungsber. Kgl. Preuss. Akad. Wiss.*, 261–267 (1924).
3. Zapf, V., Jaime, M. & Batista, C. D. Bose–Einstein condensation in quantum magnets. *Rev. Mod. Phys.* **86**, 563–614 (2014).
4. Giamarchi, T., Rüegg, C. & Tchernyshyov, O. Bose–Einstein condensation in magnetic insulators. *Nat. Phys.* **4**, 198–204 (2008).
5. Matsubara, T. & Matsuda, H. A lattice model of liquid helium, I. *Prog. Theor. Phys.* **16**, 569–582 (1956).
6. Nikuni, T., Oshikawa, M., Oosawa, A. & Tanaka, H. Bose–Einstein condensation of dilute magnons in $TlCuCl_3$. *Phys. Rev. Lett.* **84**, 5868–5871 (2000).
7. Rüegg, C. et al. Bose–Einstein condensation of the triplet states in the magnetic insulator $TlCuCl_3$. *Nature* **423**, 62–65 (2003).
8. Jaime, M. et al. Magnetic-field-induced condensation of triplons in Han purple pigment $BaCuSi_2O_6$. *Phys. Rev. Lett.* **93**, 087203 (2004).
9. Sebastian, S. E. et al. Dimensional reduction at a quantum critical point. *Nature* **441**, 617–620 (2006).
10. Zapf, V. S. et al. Bose–Einstein condensation of $S = 1$ nickel spin degrees of freedom in $NiCl_2$–$4SC(NH_2)_2$. *Phys. Rev. Lett.* **96**, 077204 (2006).
11. Batyev, E. G. & Braginskii, L. S. Antiferromagnet in a strong magnetic field: analogy with Bose gas. *Sov. Phys. JETP* **60**, 781–786 (1984).
12. Giamarchi, T. & Tsvelik, A. M. Coupled ladders in a magnetic field. *Phys. Rev.* **B59**, 11398–11407 (1999).
13. Mermin, N. D. & Wagner, H. Absence of ferromagnetism or antiferromagnetism in one- or two-dimensional isotropic Heisenberg models. *Phys. Rev. Lett.* **17**, 1133–1136 (1966).
14. Berezinskii, V. L. Destruction of long-range order in one-dimensional and two-dimensional systems possessing a continuous symmetry group. II. Quantum systems. *Sov. Phys. JETP* **34**, 610–616 (1972).
15. Kosterlitz, J. M. & Thouless, D. J. Long range order and metastability in two dimensional solids and superfluids. (Application of dislocation theory). *J. Phys. C* **5**, L124–L126 (1972).
16. Kosterlitz, J. M. & Thouless, D. J. Ordering, metastability and phase transitions in two-dimensional systems. *J. Phys. C* **6**, 1181–1203 (1973).
17. Schick, M. Two-dimensional system of hard-core bosons. *Phys. Rev. A* **3**, 1067–1073 (1971).
18. Rançon, A. & Dupuis, N. Kosterlitz–Thouless signatures in the low-temperature phase of layered three-dimensional systems. *Phys. Rev. B* **96**, 214512 (2017).
19. Hirakawa, K. Kosterlitz–Thouless transition in two-dimensional planar ferromagnet K_2CuF_4 (invited). *J. Appl. Phys.* **53**, 1893–1898 (1982).
20. Hemmida, M., Krug von Nidda, H.-A., Tsurkan, V. & Loidl, A. Berezinskii–Kosterlitz–Thouless type scenario in the molecular spin liquid ACr_2O_4(A =Mg, Zn, Cd). *Phys. Rev. B* **95**, 224101 (2017).
21. Heinrich, M., Krug von Nidda, H.-A., Loidl, A., Rogado, N. & Cava, R. J. Potential signature of a Kosterlitz–Thouless transition in $BaNi_2V_2O_8$. *Phys. Rev. Lett.* **91**, 137601 (2003).
22. Tutsch, U. et al. Evidence of a field-induced Berezinskii–Kosterlitz–Thouless scenario in a two- dimensional spin–dimer system. *Nat. Commun.* **5**, 5169 (2014).
23. Fisher, D. S. & Hohenberg, P. C. Dilute Bose gas in two dimensions. *Phys. Rev. B* **37**, 4936–4943 (1988).
24. Allenspach, S. et al. Multiple magnetic bilayers and unconventional criticality without frustration in $BaCuSi_2O_6$. *Phys. Rev. Lett.* **124**, 177205 (2020).
25. Weickert, F. et al. Low-temperature thermodynamic properties near the field-induced quantum critical point in $NiCl_2$-$4SC(NH_2)_2$. *Phys. Rev. B* **85**, 184408 (2012).
26. Sala, G. et al. Crystal field splitting, local anisotropy, and low-energy excitations in the quantum magnet $YbCl_3$. *Phys. Rev. B* **100**, 180406 (2019).
27. Xing, J. et al. Néel-type antiferromagnetic order and magnetic field-temperature phase diagram in the spin-1/2 rare-earth honeycomb compound $YbCl_3$. *Phys. Rev. B* **102**, 014427 (2020).
28. Sala, G. et al. Van hove singularity in the magnon spectrum of the antiferromagnetic quantum honeycomb lattice. *Nat. Commun.* **12**, 171 (2021).
29. Sala, G. et al. Field-tuned quantum renormalization of spin dynamics in the honeycomb lattice Heisenberg antiferromagnet $YbCl_3$. *Commun. Phys.* **6**, 234 (2023).
30. Hao, Y. et al. Field-tuned magnetic structure and phase diagram of the honeycomb magnet $YbCl_3$. *Sci. China Phys. Mech. Astron.* **64**, 237411 (2020).
31. Sengupta, P. et al. Nonmonotonic field dependence of the Néel temperature in the quasi-two-dimensional magnet $[Cu(HF_2)(pyz)_2]BF_4$. *Phys. Rev. B* **79**, 060409(R) (2009).
32. Hijmans, J. P. A. M., Kopinga, K., Boersma, F. & de Jonge, W. J. M. Phase diagrams of pseudo one-dimensional Heisenberg systems. *Phys. Rev. Lett.* **40**, 1108–1111 (1978).
33. Popov, V. N. On the theory of the superfluidity of two- and one-dimensional Bose systems. *Theor. Math. Phys.* **11**, 565–573 (1972).
34. Popov, V. N. *Functional Integrals in Quantum Field Theory and Statistical Physics* (Reidel, 1983).
35. Yamada, F. et al. Magnetic-field induced Bose–Einstein condensation of magnons and critical behavior in interacting spin dimer system $TlCuCl_3$. *J. Phys. Soc. Jpn.* **77**, 013701 (2008).
36. Matsumoto, M., Normand, B., Rice, T. M. & Sigrist, M. Magnon dispersion in the field-induced magnetically ordered phase of $TlCuCl_3$. *Phys. Rev. Lett.* **89**, 077203 (2002).
37. Paduan-Filho, A. et al. Critical behavior of the magnetization in the spin-gapped system $NiCl_2$–$4SC(NH_2)_2$. *J. Appl. Phys.* **105**, 07D501 (2009).
38. Hikami, S. & Tsuneto, T. Phase transition of quasi-two dimensional planar system. *Prog. Theor. Phys.* **63**, 387–401 (1980).
39. Cuccoli, A., Roscilde, T., Vaia, R. & Verrucchi, P. Field-induced *XY* behavior in the $S = 1/2$ antiferromagnet on the square lattice. *Phys. Rev. B* **68**, 060402(R) (2003).

https://doi.org/10.1038/s41567-024-02498-w

40. Kohama, Y. et al. Thermal transport and strong mass renormalization in $NiCl_2$-$4SC(NH_2)_2$. *Phys. Rev. Lett.* **106**, 037203 (2011).
41. Momma, K. & Izumi, F. VESTA3 for three-dimensional visualization of crystal, volumetric and morphology data. *J. Appl. Crystallogr.* **44**, 1272–1276 (2011).

Methods

Single crystals

Single-crystalline samples of $YbCl_3$ used in this study, transparent and with a thin plate-like shape, were synthesized by a self-chemical-vapour-transport method. Polycrystalline anhydrous $YbCl_3$ (Sigma-Aldrich 99.99%) was used as a starting material and sealed under vacuum in a long quartz tube with inner diameter of 15 mm. The starting material was placed at the hot end of the tube, which was heated to 900 °C and subsequently cooled down to 750 °C at a rate of 1 °C per hour. The temperature difference between the hot and the cold ends of tube was approximately 100 °C during the growth. The negligibly small paramagnetic responses from the impurities in M and the large boundary-limited κ confirm the high quality of the single crystals. The crystallographic axis was checked by single-crystal X-ray diffraction. The magnetic field was applied always along the in-plane a-axis.

Magnetization measurements

The magnetization M below 3 K was measured with a homemade Faraday magnetometer installed in a ^{3}He–^{4}He dilution refrigerator. The measurements were conducted on a few pieces of crystals put together, aligned in the same direction, with a total mass of ~0.7 mg. These were covered with dried Apiezon-N grease to protect the crystals from oxidation. The oxidation of samples could be checked by the presence of a paramagnetic response in the magnetization curve. We used data only from crystals with negligibly small traces of such response. The absolute value of M was determined by calibrating the magnitude of the field-dependent Faraday signals at 2 K with previous data taken at 1.8 K (ref. 30). The 0.2 K difference between the two measurements gives an error in the calibration up to ~1%, which does not influence the conclusion of this work. We further checked that the calibrated data are consistent with those measured at high temperatures $T \geq 2$ K by a commercial setup (Quantum Design Physical Property Measurement System, Vibrating Sample Magnetometer option).

Specific heat measurements

The specific heat C was measured by a relaxation calorimetry[42] for aligned crystals with a total mass of ~0.07 mg, which were covered with Apiezon-N grease to avoid oxidation. The total mass was determined by matching the C of single crystals with that of a polycrystalline sample at zero field and below ~1 K, where the contribution from the grease can be reasonably neglected. The grease contribution was determined as a difference from the polycrystalline sample at higher T. This amounts to 15% of the total heat capacity at 2 K and shows roughly T^2-dependence, which can be ascribed to the contribution from amorphous phonons of the grease. We subtracted this from all the data including those under fields.

Thermal conductivity measurements

κ was measured with a conventional steady-state method using a ^{3}He–^{4}He dilution refrigerator in a temperature range of 0.1–3 K. The sample with dimensions ~1 mm × ~2 mm × ~20 µm thick was mounted onto a homemade cell. The cell was sealed in a glove box under argon atmosphere, which was then evacuated in the cryostat through a simple pop-up valve mechanism. Two more samples with similar dimensions were measured using a ^{3}He cryostat, and the results were well reproduced in the T-range of overlap (0.3–3 K).

Data availability

The data that support the findings of this study are available from the corresponding authors upon reasonable request. Source data are provided with this paper.

References

42. Matsumoto, Y. & Nakatsuji, S. Relaxation calorimetry at very low temperatures for systems with internal relaxation. *Rev. Sci. Instrum.* **89**, 033908 (2018).

Acknowledgements

We acknowledge C. D. Batista, Y. Kato and D. Huang for stimulating discussions and K. Pflaum and M. Dueller for experimental support. This work was partly supported by the Alexander von Humboldt Foundation and the Japan Society for the Promotion of Science KAKAENHI (grant nos. JP22H01180 and JP17H01140) and by the Max-Planck-UBC-UTokyo Center for Quantum Materials and the Deutsche Forschungsgemeinschaft (German Research Foundation) – TRR 360 – 492547816.

Author contributions

Y.M., K.K. and H.T. conceived the research. K.K. synthesized the single crystals. Y.M. performed the magnetization and specific heat measurements. J.A.N.B., S.S. and Y.M. performed the thermal conductivity measurements. J.N. performed the structural characterization of crystals. Y.M., J.A.N.B. and H.T. analysed the data. G.J. and H.T. provided theoretical inputs. P.R. and G.J. verified the analysis. Y.M. and H.T. wrote the paper with inputs from all the authors.

Funding

Open access funding provided by Max Planck Society.

Competing interests

The authors declare no competing interests.

Additional information

Supplementary information The online version contains supplementary material available at https://doi.org/10.1038/s41567-024-02498-w.

Correspondence and requests for materials should be addressed to Yosuke Matsumoto or Hidenori Takagi.

Peer review information *Nature Physics* thanks Adam Aczel, Marcelo Jaime and the other, anonymous, reviewer(s) for their contribution to the peer review of this work.